PET Imaging of High-Affinity α4β2 Nicotinic Acetylcholine Receptors in Humans with ^{18}F-AZAN, a Radioligand with Optimal Brain Kinetics

Dean F. Wong[1–5], Hiroto Kuwabara[1], Jongho Kim[1], James R. Brašić[1], Wichana Chamroonrat[1], Yongjun Gao[1], Heather Valentine[1], William Willis[1], Anil Mathur[1], Mary E. McCaul[2], Gary Wand[2], Emily G. Gean[1], Robert F. Dannals[1], and Andrew G. Horti[1]

[1]Department of Radiology, School of Medicine, Johns Hopkins University, Baltimore, Maryland; [2]Department of Psychiatry, School of Medicine, Johns Hopkins University, Baltimore, Maryland; [3]Department of Neuroscience, School of Medicine, Johns Hopkins University, Baltimore, Maryland; [4]Environmental Health Sciences, School of Public Health, Johns Hopkins University, Baltimore, Maryland; and [5]Carey School of Business, Johns Hopkins University, Baltimore, Maryland

We evaluated (−)-2-(6-[^{18}F]fluoro-2,3′-bipyridin-5′-yl)-7-methyl-7-aza-bicyclo[2.2.1]heptane (^{18}F-AZAN), a novel radiotracer that binds to α4β2 nicotinic acetylcholine receptors (α4β2-nAChRs) and shows high specific binding and rapid and reversible kinetics in the baboon and human brain. **Methods:** We tested safety tolerability and test–retest reliability ($n = 5$) and proposed initial quantification of ^{18}F-AZAN receptors in 3 healthy human subjects who had nicotine exposure and 9 who did not. We also present a receptor blocking study in a nicotine subject dosed with the α4β2-nAChR–selective partial agonist varenicline. **Results:** Radiation dosimetry PET/CT experiments indicated that most human organs received doses between 0.008 and 0.015 mSv/MBq, with an effective dose of approximately 0.014 mSv/MBq. The tracer rapidly entered the brain, and the peak was reached before 20 min, even for thalamus. Ninety-minute scans were sufficient for ^{18}F-AZAN to obtain the ratio at equilibrium of specifically bound radioligand to nondisplaceable radioligand in tissue (BP_{ND}) using plasma reference graphical analysis, which showed excellent reproducibility of BP_{ND} (test–retest variability < 10%) in the nAChR-rich brain regions. Regional plasma reference graphical analysis BP_{ND} values exceeded 2 in the midbrain tegmental nuclei, lateral geniculate body, and thalamus for nonsmokers ($n = 9$) but were less than 1 in the nAChR-poor brain regions. There was a dramatic reduction of ^{18}F-AZAN brain uptake in smokers and varenicline-treated subjects. **Conclusion:** ^{18}F-AZAN is a highly specific, safe, and effective PET radioligand for human subjects that requires only 90 min of PET scanning to estimate high-affinity α4β2-nAChR in the living human brain.

Key Words: PET; nicotinic receptors; human neuroimaging

J Nucl Med 2013; 54:1308–1314
DOI: 10.2967/jnumed.112.108001

Nicotinic acetylcholine receptors (nAChRs) are associated with several disorders involving alteration of the density of the receptor in the central nervous system, such as Alzheimer and Parkinson diseases, schizophrenia, attention deficit hyperactivity disorder, autosomal dominant nocturnal frontal lobe epilepsy, and tobacco dependence (*1–5*).

The α4β2-nAChR is the most prominent subtype of nicotinic acetylcholine receptors in mammalian brain, with the highest density of this receptor being in the thalamus, an intermediate density in the cortical regions and caudate, and the lowest density in the cerebellum (*1,6*). Available radioligands for the quantitative PET imaging of nAChR in humans, 2-^{18}F-fluoro-3-(2(*S*)-azetidinylmethoxy)pyridine (2-^{18}F-FA) (*7*) and 6-^{18}F-fluoro-3-(2(*S*)-azetidinylmethoxy)pyridine (6-^{18}F-FA), exhibit slow distribution kinetics in primates, requiring hours of scanning (*3,8–15*). Even the bolus-plus-infusion approach, which allows a shorter scanning time, does not resolve the problem completely because of the long postinjection waiting period of more than 6 h (*16*). As a result, imaging of nAChR is logistically difficult for researchers and patients.

In contrast, we recently presented a substantially improved α4β2-nAChR radiotracer, (−)-2-(6-[^{18}F]fluoro-2,3′-bipyridin-5′-yl)-7-methyl-7-aza-bicyclo[2.2.1]heptane (^{18}F-AZAN), showing high specific uptake in the mouse brain (*17*) and high specific binding and rapid and reversible kinetics in the baboon brain (*18*). In the current study, we validated the PET properties of ^{18}F-AZAN in the human brain. Specifically, we tested whether it allows a shorter scan time (<90 min) than alternatives; whether the desired variable (the ratio at equilibrium of specifically bound radioligand to nondisplaceable radioligand in tissue [BP_{ND}] (*19*)) is accessible, has acceptable values, and is reproducible in a test–retest paradigm; and whether binding is displaced by nicotine and an α4β2-nAChR–selective partial agonist, varenicline.

MATERIALS AND METHODS

This was a single-center, open-label, nonrandomized study. The study received human subject protection approval from the Johns Hopkins School of Medicine Institutional Review Board and was conducted under a U.S. investigational new drug application after appropriate animal toxicology studies of the unlabeled ligand and

Received May 8, 2013; revision accepted Feb. 28, 2013.
For correspondence or reprints contact: Dean F. Wong, 601 N. Caroline St., JHOC Room 3245, Johns Hopkins Medical Institutions, Baltimore, MD 21287-0807.
E-mail: dfwong@jhmi.edu
Published online Jun. 25, 2013.

radiation dosimetry. All participants provided written, informed consent.

Preparation of ^{18}F-AZAN

^{18}F-AZAN was prepared as described in the literature (*17,18*). ^{18}F-AZAN was formulated as a sterile and pyrogen-free solution in saline with 8% ethanol at a pH of 5.5–6.5, with radiochemical purity greater than 99% and specific radioactivity in the range of 277–1,591 GBq/μmol (7,500–43,000 mCi/μmol) at the time synthesis ended.

Whole-Body Dosimetry

Data from mouse whole-body dissection studies provided an initial estimate of the overall safety of administration of ^{18}F-AZAN, and estimates of the whole-body and internal organ radiation of absorbed doses for retest injections were taken from the first (test) injection. Male CD-1 mice weighing 25–30 g from Charles River Laboratories were used for biodistribution studies. The animals (n = 3 per time point) were sacrificed by cervical dislocation at 5, 15, 30, 60, 120, and 240 min after injection of ^{18}F-AZAN (~2.8 MBq [75 μCi]; specific radioactivity, ~370 GBq/μmol [10,000 mCi/μmol], in 0.2 mL of saline) into a lateral tail vein. The organs were rapidly removed and dissected on ice. For the bladder assay, the external urethral meatus was tied off under ether anesthesia. The organs of interest were weighed and their radioactivity content was determined in an automated γ-counter with a counting error below 3%. Aliquots of the injectate were prepared as standards and their radioactivity content was counted along with the tissue samples. The percentage injected dose per gram of tissue was calculated, and time–activity curves for various organs were generated. The estimates of human absorbed radiation dose per organ and total dose-equivalents were calculated using OLINDA/EXM software (*20*). All experimental protocols were approved by the Animal Care and Use Committee of the Johns Hopkins Medical Institutions.

Distributions of the radioactivity in the human body were determined for 2 male subjects. After a CT scan, participants had a multiple-bed-position PET scan with a Discovery PET/CT scanner (GE Healthcare) at 4 time points over 90 min after a bolus injection of ^{18}F-AZAN. Time–activity curves of organs were submitted to OLINDA/EXM software (*20*) to obtain the radiation dose estimates for human organs. This information, along with the physiologic monitoring, allowed the complete safety of ^{18}F-AZAN administration to be assessed.

Human Brain Study

Subjects. Six men (age, 47.5 ± 7.9 y [mean ± SD]) and 9 women (37.4 ± 10.7 y) participated in the brain study. Subjects were confirmed to be nonsmoking by self-report, drug-free by urinary tests, and physically and mentally healthy by history and physical examination on the day of the scan. Six subjects (3 male and 3 female) participated in test–retest scans, about 1 mo apart. Of 8 subjects who had a single scan, 1 subject had nicotine gum on the day of the scan, 2 subjects disclosed after the scan that they had been exposed to second-hand smoke the night before the scan, and 1 subject was treated with an α4β2-nAChR–selective partial agonist, varenicline, for 12 d before the scan (days 1–3, 0.5 mg/d; days 4–7, 0.5 mg twice per day; days 8–12, 1 mg twice per day).

PET Experiments. PET studies were performed on a High-Resolution Research Tomograph (CPS Innovations, Inc.), with a spatial resolution of 2.5 mm in full width at half maximum (*21*). The subjects had a venous catheter for the radioligand injection and an arterial catheter to obtain arterial blood samples for the determination of radioactivity in plasma. Subjects were positioned in the scanner with their heads restrained with a custom-made thermoplastic mask to reduce head motion during the PET data acquisition. A 6-min transmission scan was acquired using a rotating ^{137}Cs source for attenuation correction. A dynamic PET acquisition was then performed in a 3-dimensional list mode for 90 min after an intravenous bolus injection of ^{18}F-AZAN. Radial arterial blood samples were collected at short intervals (<5 s) initially and at gradually prolonged intervals throughout the PET study. Selected blood samples taken at 0, 5, 10, 20, 30, 60, and 90 min were analyzed by high-performance liquid chromatography (HPLC) for the presence of ^{18}F-AZAN and its radioactive metabolites (*17,18*).

Reconstruction. Emission PET scans were reconstructed using the iterative ordered-subset expectation-maximization algorithm corrected for attenuation, scatter, and dead time (*22*). The radioactivity was corrected for physical decay to the injection time and rebinned to 30 dynamic PET frames of 256 (left-to-right) by 256 (nasion-to-inion) by 207 (neck-to-cranium) voxels. The schedule was four 15-s, four 30-s, three 1-min, two 2-min, five 4-min, and twelve 5-min frames. The final spatial resolution is expected to be less than 2.5 mm in full width at half maximum in 3 directions (*21*).

MR Imaging. A 3-dimensional magnetization-prepared rapid gradient echo sequence MR image of each subject was obtained for anatomic identification of the structures of interest using the following parameters: repetition time, 2,110 ms; echo time, 2.73 ms; flip angle, 8; slice thickness, 0.80 mm with zero gap; field of view, 24 × 18 cm^2; and image acquisition matrix, 288 × 320.

Volumes of Interest. Cortical volumes of interest were automatically defined using Freesurfer software (http://surfer.nmr.mgh.harvard.edu

TABLE 1
Human Radiation Dose Estimates (Adult Male Model) from CD1 Mouse Distribution Study

Target organ	Estimated dose	
	mSv/MBq	rem/mCi
Adrenals	1.23E−02	4.54E−02
Brain	4.85E−03	1.79E−02
Breasts	7.47E−03	2.76E−02
Gallbladder wall	1.42E−02	5.27E−02
Lower large intestine wall	1.62E−02	6.01E−02
Small intestine	1.35E−02	4.99E−02
Stomach wall	1.08E−02	4.01E−02
Upper large intestine wall	1.29E−02	4.78E−02
Heart wall	7.60E−03	2.81E−02
Kidneys	2.26E−02	8.38E−02
Liver	2.71E−02	1.00E−01
Lungs	6.80E−03	2.51E−02
Muscle	1.03E−02	3.80E−02
Ovaries	1.62E−02	6.01E−02
Pancreas	1.23E−02	4.57E−02
Red marrow	1.90E−02	7.02E−02
Osteogenic cells	2.23E−02	8.24E−02
Skin	7.39E−03	2.74E−02
Spleen	8.92E−03	3.30E−02
Testes	2.86E−02	1.06E−01
Thymus	9.15E−03	3.39E−02
Thyroid	9.00E−03	3.33E−02
Urinary bladder wall	1.99E−01	7.38E−01
Uterus	2.29E−02	8.49E−02
Total body	1.11E−02	4.12E−02
Effective dose equivalent	2.96E−02	1.10E−01
Effective dose	2.52E−02	9.31E−02

Data are mean, n = 3; SD ≤ 60%.

TABLE 2
Human Radiation Doses (2 Men, Whole-Body PET/CT)

Target organ	Subject 1		Subject 2	
	mSv/MBq	rem/mCi	mSv/MBq	rem/mCi
Adrenals	1.37E−02	5.07E−02	1.38E−02	5.12E−02
Brain	7.32E−03	2.71E−02	1.01E−02	3.73E−02
Breasts	1.00E−02	3.72E−02	1.01E−02	3.73E−02
Gallbladder wall	1.50E−02	5.54E−02	1.46E−02	5.39E−02
Lower large intestine wall	1.45E−02	5.36E−02	1.31E−02	4.85E−02
Small intestine	1.47E−02	5.45E−02	1.34E−02	4.97E−02
Stomach wall	1.37E−02	5.08E−02	1.31E−02	4.85E−02
Upper large intestine wall	1.45E−02	5.35E−02	1.33E−02	4.90E−02
Heart wall	1.05E−02	3.89E−02	2.30E−02	8.49E−02
Kidneys	9.47E−03	3.50E−02	1.19E−02	4.40E−02
Liver	1.57E−02	5.82E−02	1.95E−02	7.20E−02
Lungs	1.01E−02	3.72E−02	3.31E−02	1.23E−01
Muscle	1.20E−02	4.42E−02	1.12E−02	4.15E−02
Ovaries	1.49E−02	5.52E−02	1.35E−02	5.01E−02
Pancreas	1.46E−02	5.38E−02	1.44E−02	5.34E−02
Red marrow	1.14E−02	4.20E−02	1.10E−02	4.07E−02
Osteogenic cells	1.87E−02	6.94E−02	1.74E−02	6.42E−02
Skin	9.52E−03	3.52E−02	8.78E−03	3.25E−02
Spleen	1.09E−02	4.02E−02	1.81E−02	6.68E−02
Testes	1.21E−02	4.49E−02	1.09E−02	4.04E−02
Thymus	1.24E−02	4.59E−02	1.25E−02	4.64E−02
Thyroid	1.09E−02	4.03E−02	1.06E−02	3.92E−02
Urinary bladder wall	2.17E−02	8.03E−02	2.41E−02	8.91E−02
Uterus	1.53E−02	5.67E−02	1.40E−02	5.19E−02
Total body	1.22E−02	4.51E−02	1.20E−02	4.45E−02
Effective dose equivalent	1.36E−02	5.05E−02	1.70E−02	6.28E−02
Effective dose	1.28E−02	4.72E−02	1.53E−02	5.66E−02

(*23*)) and combined into standard regions including frontal, temporal, parietal, and occipital cortices, fusiform gyrus, cingulate, and insula. Subcortical regions were defined with FIRST software (http://www.fmrib.ox.ac.uk/fsl (*24*)) and manually adjusted on individual MR images. Subcortical regions included putamen, caudate nucleus, globus pallidus, thalamus, hippocampus, and amygdala. Volumes of interest were transferred from MR imaging to PET spaces following MR imaging–to–PET coregistration parameters given by SPM5 (*25*) to obtain time–activity curves of regions.

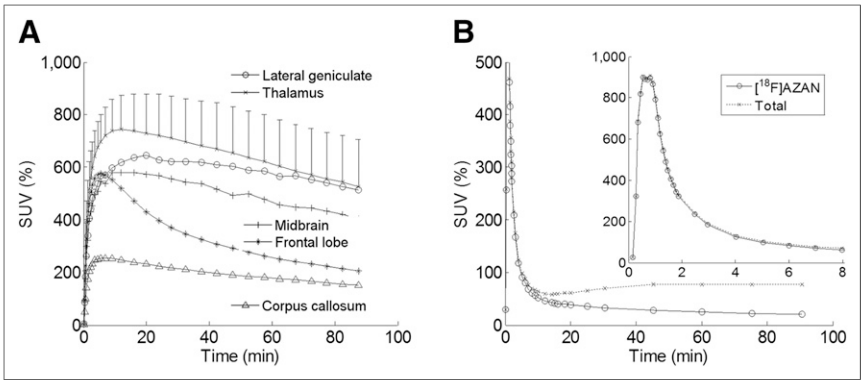

FIGURE 1. (A) Plots of time–activity curves of selected brain regions after injection of ^{18}F-AZAN expressed as percentage standardized uptake value averaged across scans of subjects without recent history of nicotine exposure (9 subjects, 14 scans). SD bars are shown for thalamus for reference. (B) Plots of total and metabolite-corrected plasma time–activity curves. Inset shows first 8 min after slow-bolus injection.

Derivation of PET Outcome Variables. A set of standard plasma input methods was used to identify the optimal method for derivation of the total volume of distribution (V_T) for ^{18}F-AZAN. The following 4 methods were tested: a 1-tissue-compartment model with 3 parameters (K_1 and k_2' (*19*) and v_0 [tissue vascular volume]), 2-tissue-compartment models (TTCMs) with 5 parameters (K_1, k_2, k_3, k_4 (*19*), and v_0) without and with constraining the K_1/k_2 ratio (nondisplaceable distribution volume, V_{ND} (*19*), to the cerebellum estimate [TTCM-C]), and the plasma reference graphical analysis (PRGA (*26*)). In TTCM and TTCM-C, BP_{ND} was given as the k_3/k_4 ratio. The Akaike information criterion was used to select the method that showed the lowest Akaike information criterion values among the 1-tissue-compartment model, TTCM, and TTCM-C. Metabolite-corrected plasma time–activity curves were obtained by applying percentage parent ligand time-profiles given by HPLC analysis to total plasma time–activity curves, after using interpolation (piecewise cubic Hermite) in Matlab (MathWorks).

To visually confirm regional differences in BP_{ND} in control subjects, and displacement of ^{18}F-AZAN binding in subjects with nicotine-exposure history and varenicline treatment, BP_{ND} maps were generated by applying PRGA on voxels, spatially normalized using parameters of PET-to-MR imaging coregistration (*25*) and MR

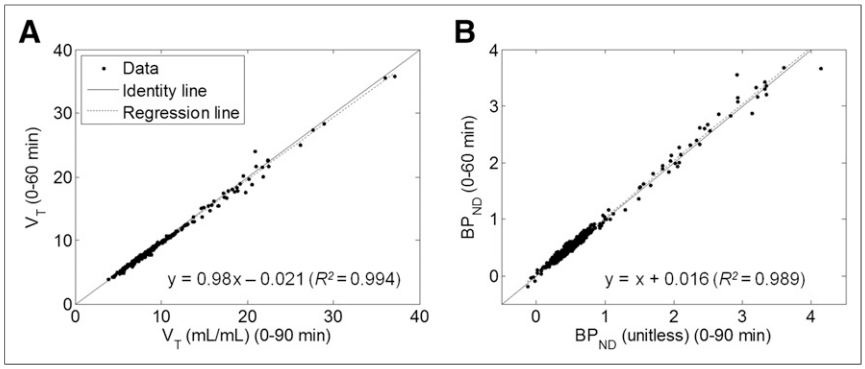

FIGURE 2. Scatterplots of regional V_T (A; using 18 scans from 13 subjects, 25 regions per scan, including corpus callosum) and BP_{ND} (B; excluding corpus callosum) given by PRGA, 0–60 min (i.e., using frames taken between 0 and 60 min after injection [y]) vs. 0–90 min (x). Regression equations are shown with coefficient of determination (R^2). $P < 0.001$ for both A and B.

imaging-to-standard MR imaging spatial normalization (SPM unified segmentation method (*25*)), and averaged across members.

Test–Retest Variability (TRV). TRV of V_T and BP_{ND} was calculated using the following equation (expressed as a percentage) to estimate the reproducibility of the PET outcome variables in individual regions:

$$TRV = |v_T - v_R|/[(v_T + v_R)/2],$$

where subscripts T and R indicate test and retest scans, respectively.

RESULTS

Whole-Body Dosimetry

In the mouse dosimetry studies, most organs received about 0.007–0.03 mSv/MBq (Table 1). The urinary bladder received the highest dose, about 0.2 mSv/MBq. This was likely an overestimate because of the procedure of bladder instrumentation. The human bladder dosimetry is the most appropriate. The effective dose was about 0.03 mSv/MBq. In the human dosimetry studies, the ^{18}F-AZAN dose for the 2 participants was 168.2 ± 20 MBq (4.55 ± 0.54 mCi), specific radioactivity was 851 ± 518 GBq/μmol (23 ± 14 Ci/μmol), mass dose was 0.07 ± 0.05 μg, and mass dose per kilogram was 0.8 ± 0.7 ng/kg. Most organs (Table 2) appeared to receive around 0.008–0.015 mSv/MBq (0.032–0.055 rem/mCi). The urinary bladder received the highest dose, around 0.023 mSv/MBq (0.085 rem/mCi). The effective dose was about 0.014 mSv/MBq (0.052 rem/mCi).

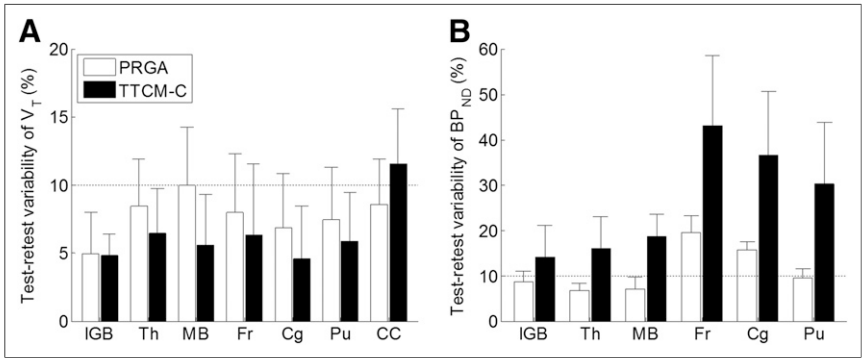

FIGURE 3. TRV (%) of V_T (A) and BP_{ND} (B) for PRGA and TTMC-C (5 subjects). Horizontal dotted lines indicate 10% TRV level for reference.

Human Brain Study

Three scans were eliminated from data analysis due to scanner ($n = 1$) or HPLC-related ($n = 2$) problems. Thus, method evaluation was performed on 18 scans from 13 subjects, test–retest evaluation was done on 5 subjects, and regional V_T and BP_{ND} values were obtained on 9 control (14 scans), 3 nicotine-exposed, and 1 varenicline-treated subjects.

Tissue and Plasma Time–Activity Curves

Injected doses of ^{18}F-AZAN ranged from 186 to 599 MBq (5.03–16.19 mCi), with specific radioactivity ranging from 128 to 1,138 GBq/μmol (3.46–30.77 Ci/μmol). Time–activity curves of selected brain regions are shown in Figure 1, expressed as average percentage standardized uptake value across subjects without a recent history of nicotine exposure. Thalamus time–activity curves peaked before 20 min after injection and then decreased monotonically. The lateral geniculate body and midbrain tegmentum nucleus, 2 regions of high uptake, showed slightly slower uptake than did the thalamus. Other cortical and subcortical regions showed rapid uptake (peaked before 10 min) and clearance, as exemplified by frontal cortex in Figure 1A. The corpus callosum showed lower accumulation of the radioactivity than did gray matter structures characterized by slow uptake and clearance. Total and metabolite-corrected plasma time–activity curves are shown as percentage standardized uptake value in Figure 1B. Total radioactive metabolites averaged (±SD) 4.4% ± 4.4% at 5 min, 24.9% ± 9.1% at 15 min, 48.4% ± 9.3% at 30 min, 64.3% ± 8.7% at 60 min, and 70.2% ± 8.5% at 90 min.

Evaluation of Data Analysis Methods

The 1-tissue-compartment model was rejected because TTCM showed lower Akaike information criterion values than the 1-tissue-compartment model in all cases. However, TTCM suffered unstable estimates of V_T and BP_{ND} (e.g., coefficients of variation > 50% in regions) compared with TTCM-C (coefficient of variance < 30%). PRGA showed excellent time consistency (0–60 min, that is, using data obtained between 0 and 60 min after injection vs. 0–90 min) on V_T and BP_{ND} estimates (Fig. 2) with t* (the start of asymptote) set at 20 min. However, TTCM-C suffered some outliers (V_T or $BP_{ND} > 40$) and showed similar time consistency to PRGA only after removal of outliers (R^2 [the coefficient of determination] = 0.994 for V_T; $R^2 = 0.948$ for BP_{ND}). The use of larger cortical regions stabilized estimates of V_{ND} (e.g., coefficient of variance decreased from 31.1% in corpus callosum to 15.3% in occipital cortex) without eliminating outliers or improving time consistency. These findings suggested that PRGA may be the optimal method for the derivation of V_T and BP_{ND} for ^{18}F-AZAN. However, TTCM-C was used for TRV calculation to confirm the findings of this section.

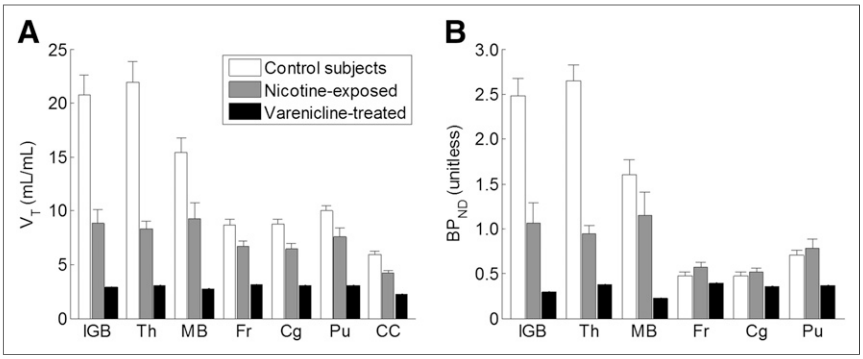

FIGURE 4. Regional V_T (A; mean boxes with SE bars) and BP_{ND} (B) of ^{18}F-AZAN given by PRGA for subjects without (control; $n = 9$) and with (nicotine-exposed; $n = 3$) recent history of nicotine, and with varenicline treatment ($n = 1$). Regions are lateral geniculate body (lGB), thalamus (Th), mid brain tegmental nucleus (MB), frontal (Fr) and cingulate (Cg) cortices, putamen (Pu), and corpus callosum (CC).

TRV

TRV estimates of selected regions are shown in Figure 3 (V_T, Fig. 3A; BP_{ND}, Fig. 3B), together with the frontal lobe to exemplify cortical regions and corpus callosum, the reference region. TRV estimates of V_T did not differ between the 2 methods, slightly below 10%, except for corpus callosum by TTCM-C. However, PRGA showed TRV estimates below 10% in high-BP_{ND} regions, a widely accepted level (*27,28*) in high-BP_{ND} regions, whereas TTCM-C showed higher TRV estimates across regions.

Regional V_T and BP_{ND}

Regional V_T and BP_{ND} values given by PRGA are shown in Figure 4 for selected brain regions. In control subjects without a recent history of nicotine exposure, the lateral geniculate body, thalamus, and midbrain tegmentum nucleus showed the highest V_T and BP_{ND} values among the 25 brain regions. Frontal and cingulate cortices, of particular importance in cognition, showed middle-range V_T and BP_{ND} among cortical regions, whereas putamen showed the highest V_T and BP_{ND} among subcortical regions. None of the subcortical regions, except for the lateral geniculate body, thalamus, and midbrain tegmentum nucleus, exhibited BP_{ND} values greater than 1. These regional differences in BP_{ND}, given by the above volume-of-interest–based analyses, were visually confirmed by spatially normalized, averaged BP_{ND} maps (Fig. 5; left column). BP_{ND} images also confirmed displacement of BP_{ND} in subjects with nicotine-exposure history and in 1 subject who received varenicline pretreatment (Fig. 5; right columns).

DISCUSSION

Because of the relatively low density of central nervous system α4β2-nAChR, the development of a quality PET radioligand for nAChRs with high specific binding and sufficiently rapid brain kinetics is a challenge. The kinetic drawbacks of existing nAChR radioligands (2-^{18}F-FA and 6-^{18}F-FA) prompted the development of radioligands with faster brain kinetics by our group and others (*8–12,14,15,29*). Studies in our labs on the radioligand structure–imaging properties relationship (*17,30–32*) led us to synthesize ^{18}F-AZAN, an α4β2-nAChR antagonist with rapid brain kinetics and high binding potential values in mice and baboons (*17,18*). Further, a blockade PET study (*18*) with the selective partial α4β2-nAChR agonist cytisine strongly suggested that ^{18}F-AZAN binds predominantly at α4β2-nAChRs. Moreover, unlike 2-^{18}F-FA, a radioligand with exceptionally low lipophilicity, ^{18}F-AZAN exhibits an optimal value of lipophilicity for blood–brain permeability (Table 3).

The baseline PET experiments in human subjects showed that ^{18}F-AZAN rapidly enters the brain and is distributed in brain regions with high densities of α4β2-nAChR. In the thalamus, a region with the greatest density of α4β2-nAChR, the radioactivity peaked at 10–15 min after injection with robust washout throughout the rest of the scanning. The uptake was more rapid in the cortex and corpus callosum, the regions with intermediate and the lowest densities of nAChR, respectively.

As expected, brain uptake of ^{18}F-AZAN was substantially lower in patients exposed to nicotine, because of competition with ^{18}F-AZAN. The accumulation of ^{18}F-AZAN radioactivity in human brain was blocked by oral preadministration of (−)-nicotine (Fig. 5). The blocking effect of nicotine was more evident in the nAChR-rich thalamus and lateral geniculate body than in the striatum and corpus callosum, confirming that ^{18}F-AZAN specifically binds at nAChR in the human brain. Blocking was also demonstrated after varenicline administration, further confirming the α4β2-nAChR in vivo specificity.

The rate of the ^{18}F-AZAN metabolism is slightly faster than that of 2-^{18}F-FA, but the metabolism rate is not likely to be a confounding factor for ^{18}F-AZAN since its scanning time is so much shorter than that used with 2-^{18}F-FA. In fact, ^{18}F-AZAN showed

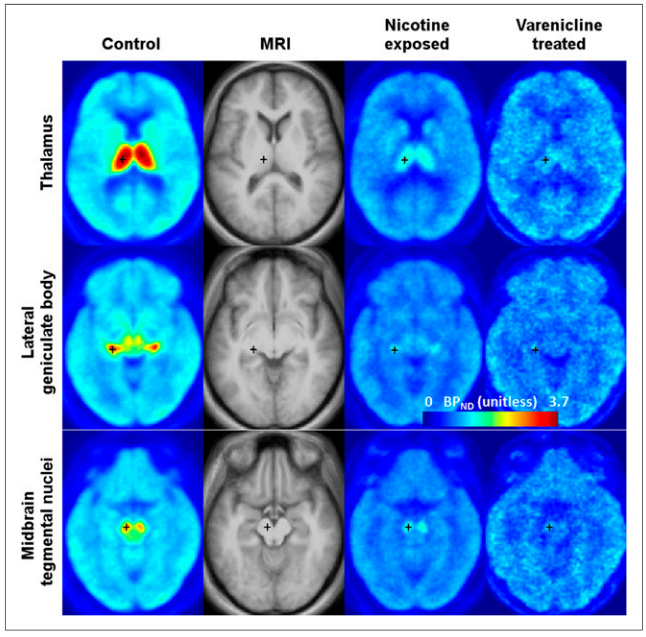

FIGURE 5. Transaxial BP_{ND} images, spatially normalized and averaged across several subjects, of ^{18}F-AZAN at levels of thalamus, lateral geniculate body, and mid brain tegmental nucleus for subjects without (control; $n = 9$) and with (nicotine-exposed; $n = 3$) recent history of nicotine, and with varenicline treatment ($n = 1$). Second column shows matching MR images.

TABLE 3
Molecular Determinants and nAChR Subtype Binding Affinity of 2-FA and AZAN (*17*)

			K_i (nM)						
Radioligand	MW (Da)	$logD_{7.4}$*	α4β2	α2β2	α2β4	α3β2	α3β4	α4β4	α6β2
2-^{18}F-FA	182	−1.4	1.33	1.44	181	3.02	3680	188	—
^{18}F-AZAN	283	1.0	0.26	0.26	7.8	4	310	6.2	0.95

MW = molecular weight.
*Experimental lipophilicity, octanol/aqueous buffer, pH 7.4.

stable regional estimates of V_T and BP_{ND} after 60 min with PRGA. In addition, the HPLC analysis demonstrated that radiometabolites of ^{18}F-AZAN are the same as those in baboon and mouse plasma and are hydrophilic and unlikely to penetrate the blood–brain barrier (*17*), which is an advantage of ^{18}F-AZAN since 2-^{18}F-FA generates a lipophilic radiometabolite in human plasma (*33*).

Evaluation of standard methods for V_T and BP_{ND} identified PRGA as the optimal method for ^{18}F-AZAN PET studies, using corpus callosum as the reference region in human subjects for BP_{ND}, as proposed for 6-^{18}F-FA (*33*) and 2-^{18}F-FA (*34*). Critical findings for this methodologic conclusion can be summarized as follows: first, this method showed time-constant estimates of V_T and BP_{ND} when the PET duration was set at 60 min or longer. Second, TRV on BP_{ND} was less than 10% in most regions, although TRV was greater than 20% for V_T. In contrast, other plasma input methods showed some negative findings. Both TTCM and TTCM-C yielded some outliers for V_T for 60- and 90-min scanning periods, although the longer scanning duration decreased outliers. BP_{ND} might not be obtained as k_3/k_4 ratio for ^{18}F-AZAN, potentially because of the fact that these methods could not identify V_{ND} (i.e., large variations of V_{ND} among subjects). Unstable estimates of V_{ND} by TTCM were also reported by other receptor radioligands such as ^{11}C-OMAR for CB1 (*35*) and ^{11}C-ABP688 for the metabotropic glutamate receptor subtype 5 (*36*). An alternative approach for BP_{ND} (i.e., [target V_T/corpus callosum V_t] − 1), which appeared successful for PRGA, resulted in high TRV values for TTCM-C because of unacceptably large TRV values on the corpus callosum. It was speculated that small errors in measurements of plasma radioactive metabolites with high metabolite percentages (i.e., >75% at 60 min) could have different effects on PRGA and compartmental analysis; the errors caused outliers and unstable estimates of V_T in the corpus callosum (the region of the lowest radioactivity) for TTCM and TTCM-C, which could be prone to errors. The errors cause higher TRV on V_T (which is directly affected by errors in plasma data) but low TRV on BP_{ND} (with plasma errors canceled out) for PRGA, assuming PRGA is robust against errors in plasma data. We specifically chose not to use the free fraction as a variable in our analysis because neither that nor blood–brain transport is directly related to our chosen outcome measures (BP_{ND} and V_T). It is also our assertion that the free fraction is a variable that can add more inaccuracy, that plasma free fraction–corrected variables are not used as commonly in the literature, and that true in vivo free fraction is controversial.

To our knowledge, only a few PET imaging studies using α4β2-nAChR radiotracers have been attempted to study important neuropsychiatric disorders such as schizophrenia (*7*) and Alzheimer disease (*37,38*), as well as smoking (*5,34,39*). ^{18}F-AZAN provides an essential tool for the expansion of imaging research in these areas.

CONCLUSION

^{18}F-AZAN allows data acquisition times of less than 1.5 h, as compared with the 6 or more hours required for the other existing human radioligands. ^{18}F-AZAN exhibits greater specific binding and is likely to be more accurate than 2-^{18}F-FA. PRGA and RTGA were identified as appropriate for obtaining BP_{ND} with ^{18}F-AZAN. With a calculated radiation dosimetry that could permit multiple studies in a single subject to be conducted, these data support ^{18}F-AZAN as an important tool for studying neuropsychiatric disorders, possible therapeutic drugs, and the effects of tobacco smoke.

DISCLOSURE

The costs of publication of this article were defrayed in part by the payment of page charges. Therefore, and solely to indicate this fact, this article is hereby marked "advertisement" in accordance with 18 USC section 1734. This work was supported by NIH grants DA020777, R33MH079017, DA026823-01, 5T32EB006351-05, R03DA027522, and K24 DA000412; SRI toxicology study M617-08; some pilot work from unrestricted funds provided by the Philip Morris USA External Research Program; and primary funding from unrestricted funds from the Johns Hopkins Department of Radiology. No other potential conflict of interest relevant to this article was reported.

ACKNOWLEDGMENTS

We thank Maria Thomas, PhD, Ayon Nandi, Stephanie Darnley, Andrew Crabb, Arman Rahmim, PhD, Hayden T. Ravert, PhD, and Daniel P. Holt for their expertise with radiotracer chemistry. We are grateful to Dr. Mike Stabin of Vanderbilt University for calculation of absorbed doses.

REFERENCES

1. Pimlott SL, Piggott M, Owens J, et al. Nicotinic acetylcholine receptor distribution in Alzheimer's disease, dementia with Lewy bodies, Parkinson's disease, and vascular dementia: in vitro binding study using 5-[^{125}I]-a-85380. *Neuropsychopharmacology.* 2004;29:108–116.
2. Holladay MW, Dart MJ, Lynch JK. Neuronal nicotinic acetylcholine receptors as targets for drug discovery. *J Med Chem.* 1997;40:4169–4194.
3. Paterson D, Nordberg A. Neuronal nicotinic receptors in the human brain. *Prog Neurobiol.* 2000;61:75–111.
4. Picard F, Bruel D, Servent D, et al. Alteration of the *in vivo* nicotinic receptor density in ADNFLE patients: a PET study. *Brain.* 2006;129:2047–2060.

5. Brody AL, Mandelkern MA, Costello MR, et al. Brain nicotinic acetylcholine receptor occupancy: effect of smoking a denicotinized cigarette. *Int J Neuropsychopharmacol.* 2009;12:305–316.
6. Lukas RJ, Changeux JP, Le Novere N, et al. International Union of Pharmacology. XX. Current status of the nomenclature for nicotinic acetylcholine receptors and their subunits. *Pharmacol Rev.* 1999;51:397–401.
7. Brašić JR, Cascella N, Kumar A, et al. Positron emission tomography (PET) experience with 2-[^{18}F]fluoro-3-(2(*S*)-azetidinylmethoxy)pyridine (2-[^{18}F]FA) in the living human brain of smokers with paranoid schizophrenia. *Synapse.* 2012;66:352–368.
8. Horti AG, Villemagne VL. The quest for Eldorado: development of radioligands for in vivo imaging of nicotinic acetylcholine receptors in human brain. *Curr Pharm Des.* 2006;12:3877–3900.
9. Gündisch D. Nicotinic acetylcholine receptors and imaging. *Curr Pharm Des.* 2000;6:1143–1157.
10. Sihver W, Langstrom B, Nordberg A. Ligands for in vivo imaging of nicotinic receptor subtypes in Alzheimer brain. *Acta Neurol Scand Suppl.* 2000;176(suppl):27–33.
11. Sihver W, Nordberg A, Langstrom B, et al. Development of ligands for in vivo imaging of cerebral nicotinic receptors. *Behav Brain Res.* 2000;113:143–157.
12. Volkow ND, Ding YS, Fowler JS, Gatley SJ. Imaging brain cholinergic activity with positron emission tomography: its role in the evaluation of cholinergic treatments in Alzheimer's dementia. *Biol Psychiatry.* 2001;49:211–220.
13. Ding YS, Fowler JS, Logan J, et al. 6-[^{18}F]fluoro-A-85380, a new PET tracer for the nicotinic acetylcholine receptor: studies in the human brain and in vivo demonstration of specific binding in white matter. *Synapse.* 2004;53:184–189.
14. Horti AG, Wong DF. Clinical perspective and recent development of PET radioligands for imaging cerebral nicotinic acetylcholine receptors. *PET Clin.* 2009; 4:89–100.
15. Horti AG, Gao Y, Kuwabara H, Dannals RF. Development of radioligands with optimized imaging properties for quantification of nicotinic acetylcholine receptors by positron emission tomography. *Life Sci.* 2010;86:575–584.
16. Kimes AS, Chefer SI, Matochik JA, et al. Quantification of nicotinic acetylcholine receptors in the human brain with PET: bolus plus infusion administration of 2-[^{18}F]F-A85380. *Neuroimage.* 2008;39:717–727.
17. Gao Y, Kuwabara H, Spivak CE, et al. Discovery of (−)-7-methyl-2-exo-[3′-(6-[^{18}F]fluoropyridin-2-yl)-5′-pyridinyl]-7-azabicyclo[2.2.1]heptane, a radiolabeled antagonist for cerebral nicotinic acetylcholine receptor (alpha4beta2-nAChR) with optimal positron emission tomography imaging properties. *J Med Chem.* 2008;51:4751–4764.
18. Kuwabara H, Wong DF, Gao Y, et al. PET imaging of nicotinic acetylcholine receptors in baboons with ^{18}F-AZAN, a radioligand with improved brain kinetics. *J Nucl Med.* 2012;53:121–129.
19. Innis RB, Cunningham VJ, Delforge J, et al. Consensus nomenclature for in vivo imaging of reversibly binding radioligands. *J Cereb Blood Flow Metab.* 2007;27:1533–1539.
20. Stabin MG, Sparks RB, Crowe E. OLINDA/EXM: the second-generation personal computer software for internal dose assessment in nuclear medicine. *J Nucl Med.* 2005;46:1023–1027.
21. Sossi V, de Jong HWAM, Barker WC, et al. The second generation HRRT: a multi-centre scanner performance investigation. *IEEE Nucl Sci Sym Conf Record.* 2005;4:2195–2199.
22. Rahmim A, Cheng JC, Blinder S, Camborde ML, Sossi V. Statistical dynamic image reconstruction in state-of-the-art high-resolution PET. *Phys Med Biol.* 2005;50:4887–4912.
23. Fischl B, van der Kouwe A, Destrieux C, et al. Automatically parcellating the human cerebral cortex. *Cereb Cortex.* 2004;14:11–22.
24. Patenaude B, Smith SM, Kennedy DN, Jenkinson M. A Bayesian model of shape and appearance for subcortical brain segmentation. *Neuroimage.* 2011;56:907–922.
25. Ashburner J, Friston KJ. Rigid body registration. In: Frackowiak RSJ, Friston KJ, Frith C, et al., eds. *Human Brain Function.* 2nd ed. Oxford, U.K.: Academic Press; 2003:635–654.
26. Logan J, Fowler JS, Volkow ND, et al. Graphical analysis of reversible radioligand binding from time-activity measurements applied to [N-^{11}C-methyl]-(−)-cocaine PET studies in human subjects. *J Cereb Blood Flow Metab.* 1990; 10:740–747.
27. Kim JS, Ichise M, Sangare J, Innis RB. PET imaging of serotonin transporters with [^{11}C]DASB: test-retest reproducibility using a multilinear reference tissue parametric imaging method. *J Nucl Med.* 2006;47:208–214.
28. Hirvonen J, Johansson J, Teräs M, et al. Measurement of striatal and extrastriatal dopamine transporter binding with high-resolution PET and [^{11}C]PE2I: quantitative modeling and test-retest reproducibility. *J Cereb Blood Flow Metab.* 2008;28:1059–1069.
29. Ding YS, Fowler J. New-generation radiotracers for nAChR and NET. *Nucl Med Biol.* 2005;32:707–718.
30. Gao Y, Horti AG, Kuwabara H, et al. Derivatives of (−)-7-methyl-2-(5-(pyridinyl)pyridin-3-yl)-7-azabicyclo[2.2.1]heptane are potential ligands for positron emission tomography imaging of extrathalamic nicotinic acetylcholine receptors. *J Med Chem.* 2007;50:3814–3824.
31. Zhang Y, Pavlova OA, Chefer SI, et al. 5-substituted derivatives of 6-halogeno-3-((2-(S)-azetidinyl)methoxy)pyridine and 6-halogeno-3-((2-(S)-pyrrolidinyl) methoxy)pyridine with low picomolar affinity for a4b2 nicotinic acetylcholine receptor and wide range of lipophilicity: potential probes for imaging with positron emission tomography. *J Med Chem.* 2004;47:2453–2465.
32. Brown LL, Kulkarni S, Pavlova OA, et al. Synthesis and evaluation of a novel series of 2-chloro-5-((1-methyl-2-(S)-pyrrolidinyl)methoxy)-3-(2-(4-pyridinyl) vinyl) pyridine analogues as potential positron emission tomography imaging agents for nicotinic acetylcholine receptors. *J Med Chem.* 2002;45:2841–2849.
33. Sorger D, Becker GA, Patt M, et al. Measurement of the α4β2* nicotinic acetylcholine receptor ligand 2-[^{18}F]fluoro-A-85380 and its metabolites in human blood during PET investigation: a methodological study. *Nucl Med Biol.* 2007; 34:331–342.
34. Mukhin AG, Kimes AS, Chefer SI, et al. Greater nicotinic acetylcholine receptor density in smokers than in nonsmokers: a PET study with 2-^{18}F-FA-85380. *J Nucl Med.* 2008;49:1628–1635.
35. Wong DF, Kuwabara H, Horti AG, et al. Quantification of cerebral cannabinoid receptors subtype 1 (CB1) in healthy subjects and schizophrenia by the novel PET radioligand [^{11}C]OMAR. *Neuroimage.* 2010;52:1505–1513.
36. Ametamey SM, Treyer V, Streffer J, et al. Human PET studies of metabotropic glutamate receptor subtype 5 with ^{11}C-ABP688. *J Nucl Med.* 2007; 48:247–252.
37. Ellis JR, Villemagne VL, Nathan PJ, et al. Relationship between nicotinic receptors and cognitive function in early Alzheimer's disease: a 2-[^{18}F]fluoro-A-85380 PET study. *Neurobiol Learn Mem.* 2008;90:404–412.
38. Kadir A, Almkvist O, Wall A, Långström B, Nordberg A. PET imaging of cortical ^{11}C-nicotine binding correlates with the cognitive function of attention in Alzheimer's disease. *Psychopharmacology (Berl).* 2006;188: 509–520.
39. Lotfipour S, Mandelkern M, Alvarez-Estrada M, Brody A. A single administration of low-dose varenicline saturates α4β2* nicotinic acetylcholine receptors in the human brain. *Neuropsychopharmacology.* 2012;37:1738–1748.